

Temperature Sensitivity of 1.54- μm Vertical-Cavity Lasers with an InP-Based Bragg Reflector

Stefan Rapp, Joachim Piprek, *Member, IEEE*, Klaus Streubel, Janos André, and J. Wallin

Abstract—We fabricated 1.54- μm laser diodes that employ one integrated GaInAsP–InP and one Si–SiO₂ mirror in combination with a strain-compensated GaInAsP multiquantum-well active layer. Considerable care has to be taken of the temperature performance of the devices. Here, an important parameter is the gain offset between the gain peak wavelength and the cavity resonance. This offset is related to the experimentally accessible photoluminescence (PL) offset between the PL-peak wavelength and the emission wavelength. Vertical-cavity laser (VCL) characteristics such as threshold current and quantum efficiency show an extremely sensitive dependence on this parameter. In this paper, we focus on the temperature performance of our VCL's as a function of the cavity tuning. VCL's designed for PL-offset values between +17 and –16 nm are fabricated and characterized. As expected, the threshold current of all lasers shows a pronounced minimum at low temperatures. The position of this minimum depends on the offset at room temperature (RT) as a parameter. However, it turns out that the minimum threshold current is not obtained by matching gain peak and cavity wavelength for that temperature. The observed behavior is described well by calculations, taking into account the temperature dependence of the optical gain, of the cavity resonance, and of the cavity losses. The model is a valuable tool to tune the lasers for example low threshold current or reduced temperature sensitivity.

Index Terms—Gain control, laser thermal factors, laser tuning, modeling, semiconductor lasers, temperature, thermal variables measurement.

I. INTRODUCTION

SINCE the first CW room-temperature operating devices were fabricated [1], long-wavelength vertical-cavity lasers (VCL's) have gained considerable interest. As a potential next-generation light source for future optical communication systems, they offer a variety of advantages such as cost-effective fabrication, on-chip-testability, array fabrication, and effective fiber coupling.

For these applications, as low as possible threshold currents and high output power are desirable. Therefore, big effort has to be put into the design of the devices. The device performance of long-wavelength (1.3–1.55 μm) laser diodes shows a strong temperature dependence, especially of the threshold current [2]. This is due to carrier leakage across the quantum wells (QW's), high nonradiative losses as Auger recombination and intervalence band absorption (IVBA) [3].

Manuscript received February 11, 1997; revised June 18, 1997. This work was supported by the European ACTS-VERTICAL Project.

S. Rapp, K. Streubel, and J. André are with the Royal Institute of Technology, Department of Electronics, 164 40 Kista, Sweden.

J. Piprek is with the University of Delaware, Newark DE 19716-3106 USA.

J. Wallin is with Ericsson Components, 16440 Kista, Sweden.

Publisher Item Identifier S 0018-9197(97)07070-X.

The temperature dependence of Fabry–Perot edge emitters is characterized by the parameter T_0 . It is deduced by assuming the lasing mode always matches the gain peak wavelength. Since the mode spacing is small compared to the linewidth of the gain, we usually find a cavity mode λ_e close to the gain peak wavelength λ_p . This holds for any temperature. In the case of VCL, the parameter T_0 has to be used carefully, since the mode spacing is large and there is usually only one mode in the range of the gain linewidth. Varying the temperature leads to an offset of gain/photoluminescence (PL) peak wavelength and cavity mode. Especially at low temperatures, this fact leads to an increase in threshold current and the behavior of $I_{\text{thr}}(T)$ is considerably different from edge emitters [4]–[7]. Here, the mismatch between PL-peak wavelength and the cavity mode dominates the temperature sensitivity. For this reason, T_0 is only a meaningful parameter for the $I_{\text{thr}}(T)$ characteristics within a specified temperature range.

In this paper, we investigate the influence of the temperature on the laser performance, especially on the threshold current showing a minimum for a particular temperature. In order to reach low threshold current and high output power, the right choice of active material and cavity design of the device are essential. Once this is fixed, it is important to realize the optimal gain offset $\lambda_p - \lambda_e$ between the gain-peak wavelength λ_p and the cavity mode λ_e (cavity resonance). The gain offset is close to the PL offset $\lambda_{\text{PL}} - \lambda_e$, where λ_{PL} is the peak wavelength of the PL. Though this requirement seems to be easy to match, it turns out as a crucial issue depending on the particular design of the active layer, p-cladding, etc., since during operation of the laser (even pulsed) this condition cannot be maintained easily. The heating of the active layer and the power dissipated in the cavity result in a shift of the PL/gain-peak as well as of the cavity mode. The latter is only important for CW operation, since the cavity does not heat under pulsed operation. We analyze the pulsed output characteristics of 1.54- μm VCL's, based on an InP–GaInAsP integrated bottom mirror. This design offers full-wafer-scale fabrication, in contrast to the successfully operating wafer fused devices [1], [8]. Lasers with a varying offset between cavity mode and PL are fabricated and the threshold current for different temperatures is recorded. The results are compared to numerical simulations.

II. DEVICE DESIGN AND FABRICATION

Fig. 1 shows the fabricated 1.54- μm VCL structure. It is a low mesa structure, which is intended for pulsed operation at room temperature (RT). No regrowth is employed. The

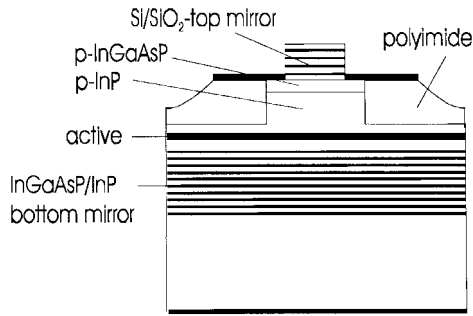


Fig. 1. VCL structure with a 50-period InGaAsP–InP integrated bottom mirror, strain-compensated MQW active and $5 \times \text{Si-SiO}_2$ top mirror. Layer parameters are given in Table II.

aim is to provide input parameters for an improved structure for CW RT operation. A detailed description of design and characteristics is given in [9]. The device is fabricated in two growth steps, using low-pressure metal organic vapor deposition (LP-MOCVD). The first growth step is the bottom mirror, consisting of 50 pairs of n-type (Si) GaInAsP–InP quarter-wavelength-thick layers, with a nominal plane-wave reflectivity of 99.9%. In a second step, the active region of nine compressively (+1% cs) strained 7-nm-thick GaInAsP QW's and strain-compensating (–0.9% ts) 8-nm-thick GaInAsP barriers is grown. The active region is grown with a constant As–P ratio in order to improve interface quality and reduce the susceptibility for temperature induced diffusion. Details about the multiquantum-well (MQW) structure and the growth procedure are described elsewhere [10]. The Zn-doped p-cladding InP and p^+ -GaInAsP ($1.3 \mu\text{m}$) contact layers are 1.95 and $0.15 \mu\text{m}$ thick, resulting in a cavity length of 4.5λ .

To determine the PL spectrum of the QW structure properly, a reference piece without underlying mirror is grown. This is done in the same run as the active region of the lasers. This is of particular importance, since the PL of the active material on top of the mirror is always modulated by the cavity which is formed between the mirror and the semiconductor–air interface on top of the structure. For this reason, it is impossible to determine the peak position of the PL properly without a reference piece. Thus, the PL peak wavelength λ_{PL} is roughly tuned to the desired PL offset; confirmed by the narrow, cavity-enhanced emission of the as-grown wafer. For the fine tuning, at this stage, the spectral position of the cavity mode can be corrected by controlled thinning (reactive ion etching, RIE) of the contact layer. Etching steps of around 15 nm are performed (see Fig. 2). For the laser processing, circular $1.6\text{-}\mu\text{m}$ -high mesas with diameters between 5 and $22 \mu\text{m}$ are etched and embedded in polyimide. The processing is concluded by the deposition of a five-period Si–SiO₂ mirror with a diameter between 3 and $20 \mu\text{m}$. The actual cavity mode position at this stage is given by the emission line of the lasers.

III. ACTIVE LAYER ANALYSIS

Since gain calculations are very sensitive on the $\text{Ga}_x\text{In}_{1-x}\text{As}_y\text{P}_{1-y}$ MQW layer compositions and thicknesses (neither of them is precisely known), parameter adjustments

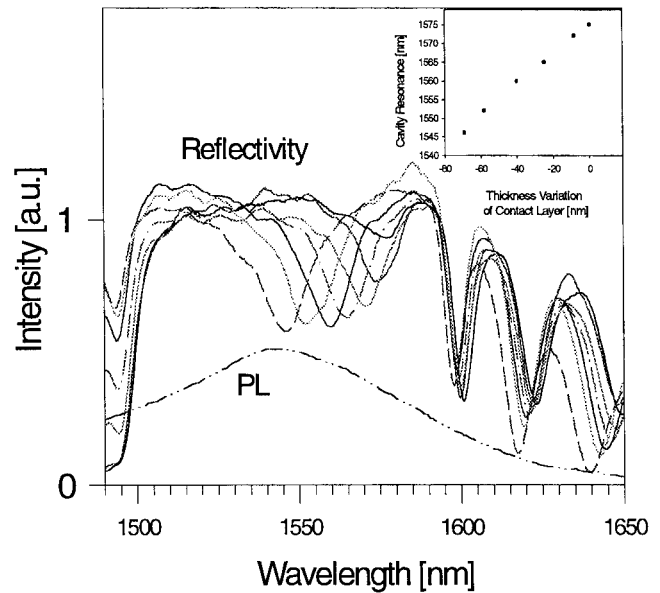


Fig. 2. Controlled thinning of contact layer and related shift of cavity resonance before deposition of the top mirror.

TABLE I
PARAMETERS FOR BEST AGREEMENT BETWEEN
RECORDED AND SIMULATED HRXD SPECTRUM

	Ga fraction x	As fraction y	thickness (nm)
well	0.774	0.78 (0.83)	7.0 (7.0)
barrier	0.536	0.78	8.6 (8.0)

The nominal values are given in parentheses.

are required to find agreement with experimental characteristics. For the present structure with a constant As–P ratio, there are five free MQW parameters: the thickness of well and barrier, l_z and l_b , and four composition parameters (x_{well} , y_{well} , x_{barr} , and y_{barr}) for both well and barriers, where $y_{\text{well}} = y_{\text{barr}}$. Using high-resolution X-ray diffraction (HRXD), the number of free parameters can be reduced to three by determination of the MQW period $l_z + l_b$ to 15.6 nm and of –0.0174% net strain. Additionally, the peak wavelength of the PL spectrum is measured at 1540 nm at RT, leaving two unknown parameters. Thus, the X-ray diffraction pattern is simulated for different As contents and QW thickness and compared to the experimentally recorded spectrum. The set of parameters for best agreement between measurement and simulation (as shown in Fig. 3) is given in Table I. While the QW thickness agrees well with the intended number, the As content is considerably smaller than intended.

The computation of the band structure using the values given in Table I shows that due to strain compensation, light holes experience almost no quantum confinement. The MQW band gap is $E_g = 805 \text{ meV}$ at RT and the calculated PL peak occurs at 1540 nm. The energy distance from the lowest QW states to the barrier band edges is relatively small (42 meV for electrons and 93 meV for heavy holes), and a considerable amount of MQW carriers can be assumed outside the QW's at high injection. On the other hand, the distance of these QW

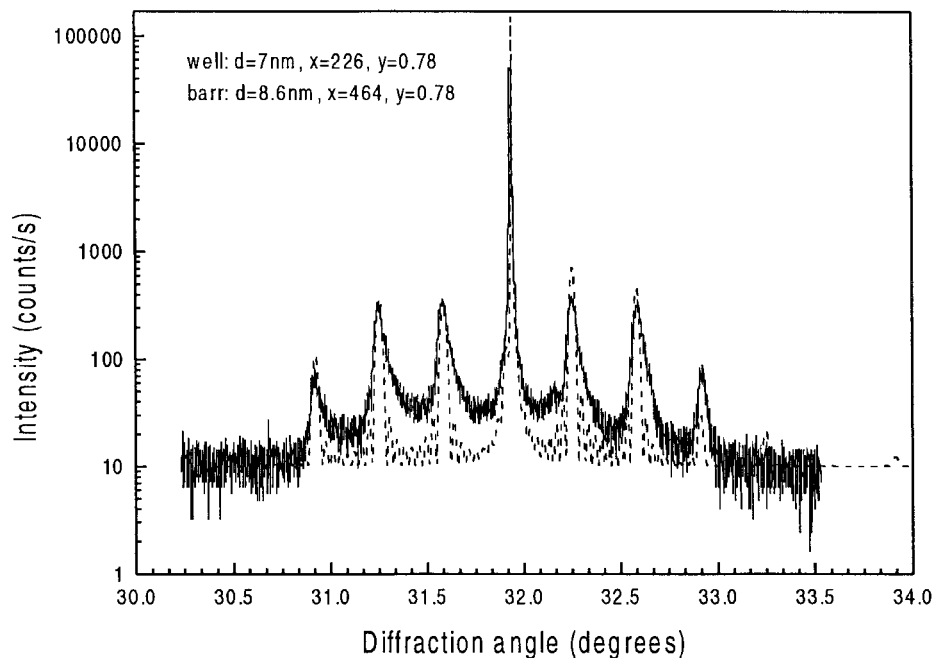


Fig. 3. Recorded (solid line) and simulated (dashed line) HRXD-pattern for the MQW, yielding the compositions shown in Table I.

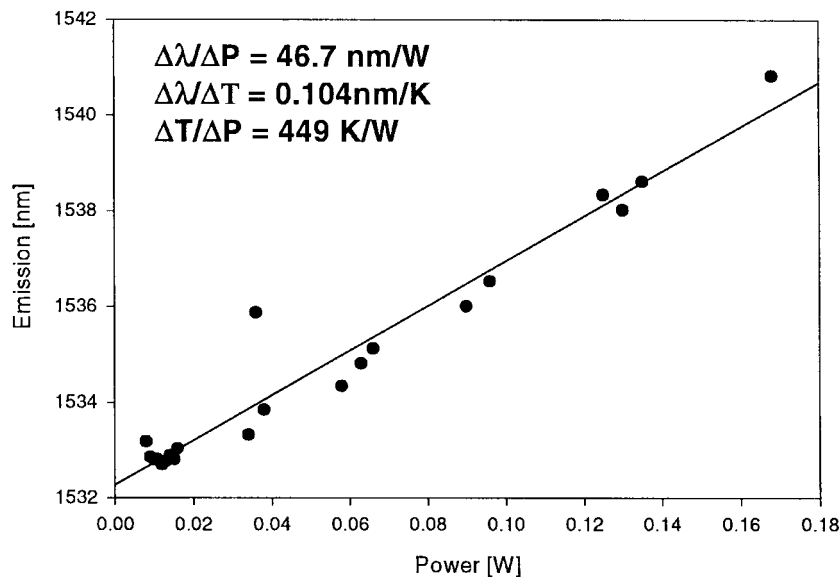


Fig. 4. Thermal resistance: emission wavelength depending on input power, measured at a temperature of -35°C .

states to the InP spacer band edges is relatively large (241 and 302 meV, respectively) and no significant carrier escape rate from the MQW is expected at RT.

IV. OPERATING CHARACTERISTICS

Pulsed RT operation is achieved for devices with top mesa diameters of 10, 15, and 20 μm at threshold currents of 70, 30, and 61 mA, respectively, corresponding to current densities of 62, 13, and 16 kA/cm^2 . These high-threshold current densities are most likely explained by a surface leakage channel along the mesas, caused by defect-induced (RIE) nonradiative recombination. Other indications for this leakage are a low external quantum efficiency as well as a small

temperature rise in the active region (Fig. 4). According to numerical simulations, the CW active region heating is expected to be three times higher than measured (Fig. 4), indicating that a large part of the heat power is generated far away from the active region.

Slightly above threshold, the lasers operate single mode. At higher current (1.5–2 times threshold) a second or third mode appears. The linewidth is less than 0.1 nm, limited by the resolution of the spectrum analyzer. For a 15- μm device, the differential resistance at threshold is 18 Ω , and the threshold voltage is 1.8 V. The lasers are investigated within the ambient temperature range of -160°C to $+42^{\circ}\text{C}$, where the characteristics improve toward lower temperatures.

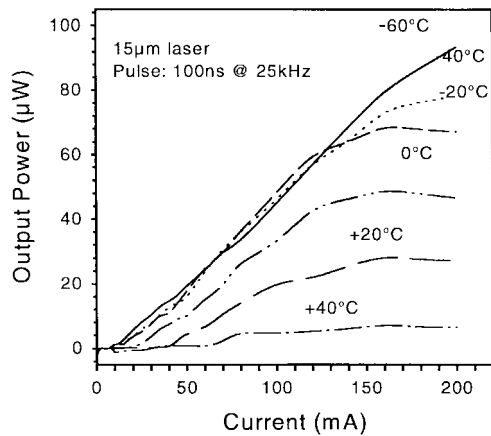


Fig. 5. Typical output characteristics of a 15- μm laser for a set of temperatures.

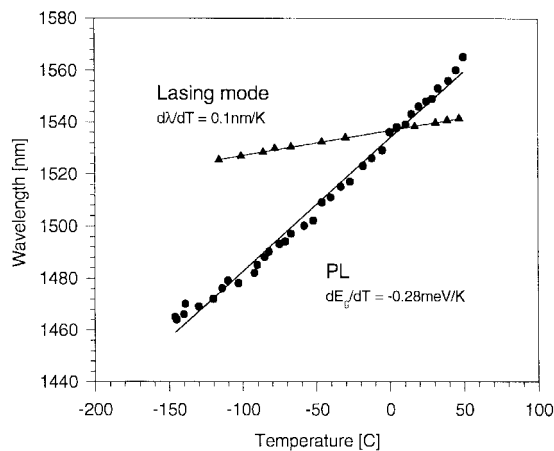


Fig. 6. Variation of cavity mode and PL, respectively, with temperature. At RT, the gain peak is 8 nm above the PL.

Typical output characteristics for several temperatures are shown in Fig. 5. CW operation is achieved at temperatures up to -25°C , even though the lasers are not designed for CW. The following analysis is done for lasers with 15- μm mesa diameter and assumes pulsed operation at different ambient temperatures. Self-heating of the laser is neglected.

V. TEMPERATURE EFFECTS

For further investigations, the temperature dependence of the PL (bandgap) and the laser line (cavity) are determined. This is of importance since, unlike in Fabry-Perot edge-emitters, in VCL's the emission wavelength λ_e is not given by the gain peak wavelength. This causes a gain offset $\lambda_p - \lambda_e$ for VCL, depending on design and temperature.

A. Energy Band Gap

Fig. 6 shows the the PL peak wavelength λ_{PL} as a function of temperature. For the investigated VCL, the PL peak at different ambient temperatures shifts by -0.54 nm/K , resulting in $dE_g/dT = -0.28\text{ meV/K}$.

TABLE II
PARAMETERS OF THE VCL LAYER THICKNESS, LAYER DOPING N_{dop} , REFRACTIVE INDEX n , AND ABSORPTION COEFFICIENT α

Parameter	layer thckn. [nm]	N_{dop} [cm^{-3}]	Refr. index	α [cm^{-1}]
Top-DBR: Si	107		3.61	400
Top-DBR: SiO ₂	267		1.45	
p-InGaAsP (1.3 μm)	302	$1 \cdot 10^{19}$	3.46	240
p-InP	1755	$1 \cdot 10^{18}$	3.17	24
In _{0.774} Ga _{0.226} As _{0.78} P _{0.22} (QW)	7		3.5	54
In _{0.536} Ga _{0.464} As _{0.78} P _{0.22} (bar)	8.6		3.5	54
n-InP	166	$5 \cdot 10^{18}$	3.17	8
n-InP (DBR)	122	$5 \cdot 10^{18}$	3.17	8
n-InGaAsP (1.4 μm , DBR)	112	$5 \cdot 10^{18}$	3.46	8
n-InP (substrate)	450	$5 \cdot 10^{18}$	3.17	8

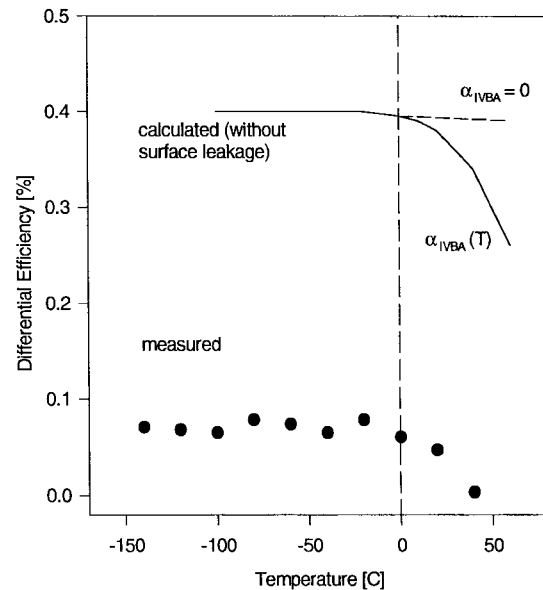


Fig. 7. Calculated and measured differential optical efficiency as function of temperature with and without IVBA.

B. Cavity Mode

With increasing temperature, the cavity mode λ_e red-shifts due to the temperature dependence of the refractive index dn/dT and layer thickness. dn/dT is assumed to be $2 \cdot 10^{-4}\text{ K}^{-1}$ for the semiconductor, $1 \cdot 10^{-4}\text{ K}^{-1}$ for Si, and $1 \cdot 10^{-5}\text{ K}^{-1}$ for SiO₂. The measurement yields $d\lambda_e/dT = 0.1\text{ nm/K}$ (Fig. 6), which is in agreement with previous results. This number as well as the emission wavelength $\lambda_e = 1538\text{ nm}$ is reproduced in the simulation later on, applying the material parameters dn/dT given above. Thus, the cavity wavelength $\lambda_e(T)$ red-shifts about six times slower than the PL peak $\lambda_{\text{PL}}(T)$ with rising temperature.

C. Differential Quantum Efficiency

Another optical parameter that can be measured easily is the differential quantum efficiency $\eta_d = \eta_i \eta_{\text{opt}}$ with the injection efficiency η_i accounting for carrier losses. Since η_d is a differential quantity, η_i is affected only by the changes in carrier losses above threshold. The value of η_{opt} is determined by optical losses within the cavity, i.e., by absorption, emission, and scattering [11]. Assuming typical absorption coefficients (Table II), a value of $\eta_{\text{opt}} = 0.4\%$ is calculated (Fig. 7)

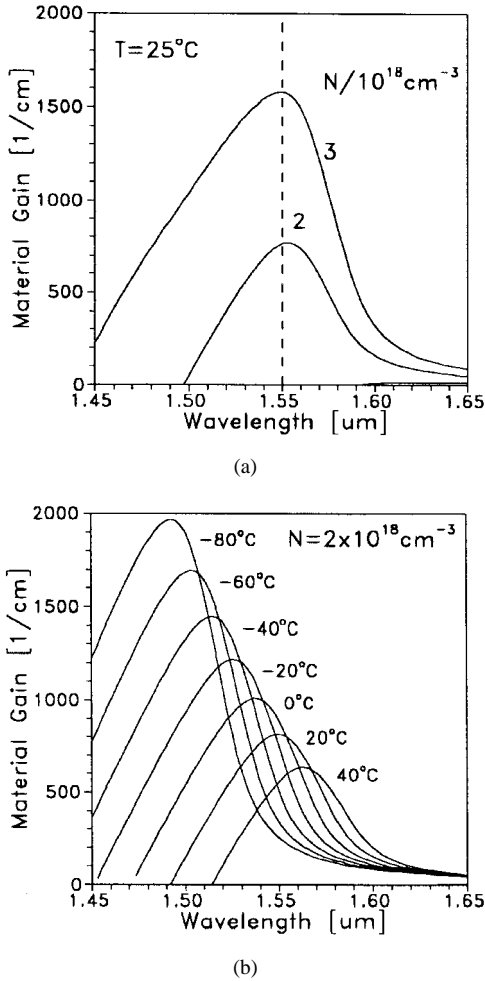


Fig. 8. (a) Calculated spectrum of the MQW optical gain with the carrier density as a parameter. The intended lasing wavelength (dashed line) is matched perfectly at room temperature. (b) MQW gain spectrum at different ambient temperatures showing the thermal shift of the peak wavelength λ_p as well as of the peak height g_{\max} .

that is much higher than the measured value $\eta_d = 0.04\%$. No reasonable change of internal optical loss parameters allows for a reduction of η_{opt} by a factor of 10. Thus, injection losses seem to be large, as expected from the high threshold current density measured. As above for the thermal resistance, it is concluded that leakage currents at the mesa surface are substantial in these devices. Such leakage currents increase with higher total current and hence reduce η_i . The differential efficiency also depends on the temperature, caused by changes in the refractive indices as well as in the absorption coefficients. In particular, IVBA within the MQW or within other layers with high hole concentration could reduce the quantum efficiency at higher temperatures [2]. This is shown in Fig. 7, comparing simulation results with and without IVBA. In the measurements, a similarly strong reduction of $\eta_d(T)$ is observed above 0°C , indicating the influence of IVBA in the VCL's.

VI. OPTICAL GAIN

Using the parameters of the active layer as well as the values for the temperature shift of bandgap and cavity mode,

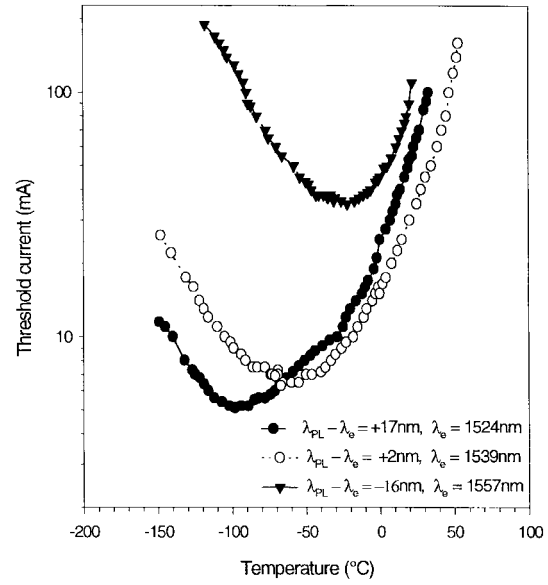


Fig. 9. Measured threshold current for three different RT-PL offsets as a function of ambient temperature.

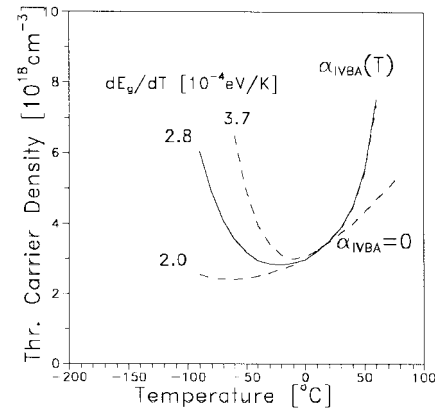


Fig. 10. Threshold carrier density as function of temperature with and without IVBA and for different parameters dE_g/dT of the thermal bandgap shrinkage.

the material gain $g(\lambda, N, T)$ is calculated as a function of wavelength, temperature, and carrier density. The gain model is based on Fermi's golden rule and 4×4 **kp** band structure computations for the strain-compensated MQW active region [12]. Fig. 8(a) shows the gain spectrum calculated for different temperatures. At RT, the gain peak wavelength λ_p is located 8 nm above the PL peak wavelength λ_{PL} . The shift of the gain peak $d\lambda_p/dT = 0.59$ nm/K is slightly faster than for the PL peak due to different carrier statistics. The height g_{\max} of the gain peak also shifts with temperature almost linearly by $dg_{\max}/dT = -11$ $\text{cm}^{-1}\text{K}^{-1}$ [Fig. 8(b)]. This is caused by the increased spreading of the carrier's Fermi distribution with rising temperature. At constant splitting of the quasi-Fermi levels of electrons and holes $\Delta E_F = F_n - F_p$, the total carrier density N would also rise with higher temperature. To keep N constant in Fig. 8(b), ΔE_F is reduced by -0.56 meV/K with increasing temperature (25°C : $\Delta E_F = 828$ meV, $F_n - E_c = 58$ meV, $E_v - F_p = -14$ meV).

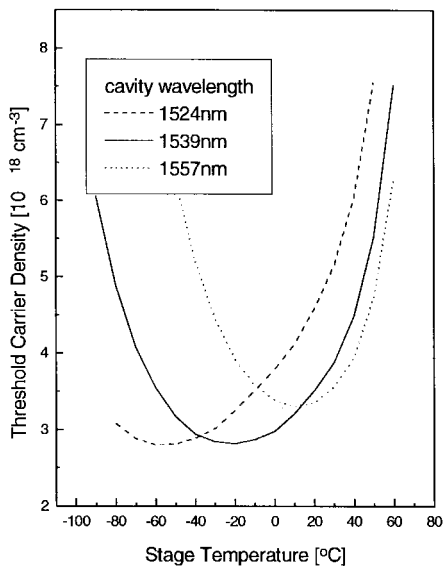


Fig. 11. Threshold carrier density as function of temperature for different cavity wavelengths (solid lines in Figs. 11 and 10 are identical).

VII. GAIN OFFSET AND THRESHOLD CURRENT

The measured emission wavelength changes slightly with the VCL position due to inhomogeneous layer thicknesses across the InP wafer. Employing these variations, the pulsed threshold current is measured against temperature at different cavity wavelengths (Fig. 9). The minimum threshold current occurs at different temperatures because of the different RT gain offset. Thus, finding the proper RT gain offset allows for the design of the threshold current temperature sensitivity.

To study the effect of the gain offset in more detail, numerical simulation is applied [13]. Here, we take into account a particular RT gain offset of +10 nm (i.e., a PL offset of +2 nm), corresponding to the curve in Fig. 9 showing the minimum at -60 °C. Firstly, the transfer matrix method is employed to obtain emission wavelength λ_e , threshold gain g_{th} , and differential optical efficiency η_{opt} as a function of the ambient temperature (cf. Figs. 6 and 7). For verification of the input parameters, the room temperature value of $\lambda_e = 1538$ nm and $d\lambda_e/dT = 0.1$ nm/K are in very good agreement with the measurement. In a second step, MQW gain calculations are performed for any given wavelength and temperature, leading to the threshold carrier density N_{th} as function of the temperature (solid curve in Fig. 10). The calculation shows a minimum at -30 °C and not near 0 °C, where a perfect match of mode and gain peak exists. This can be explained as follows: when the gain offset $\lambda_p - \lambda_e$ is increased by lowering the temperature, an increase in gain occurs for the same carrier density [Fig. 8(b)], i.e., the same gain is reached with a lower carrier density. Within a certain temperature range, this effect overcomes the mismatch of gain peak and cavity mode. The threshold carrier density *drops* despite the fact that the tuning of the laser becomes worse for lower temperature. Only for large temperature reduction, the gain drops for $N = \text{const}$. The mismatch becomes dominant, and the threshold carrier density increases again.

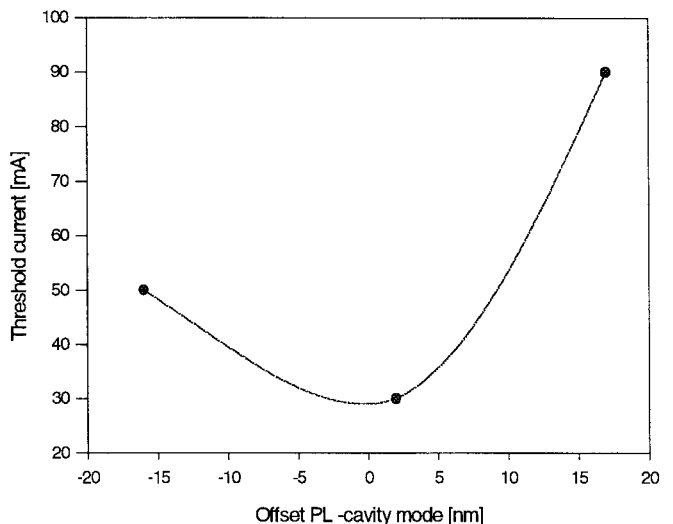


Fig. 12. Measured threshold current as a function of detuning, i.e., offset between PL and cavity mode.

In other words, to maintain a given threshold gain g_{th} required for lasing, the threshold carrier density $N_{th}(T)$ is minimum for a gain offset toward smaller wavelength, i.e., for $\lambda_p - \lambda_e < 0$. This finding is in contrast to a widely used VCL design rule saying that the gain offset must be zero for minimum threshold current $I_{thr}(T)$ [7], [14].

Fig. 10 also shows the impact of the parameter dE_g/dT on the position of the minimum as well as the influence of IVBA (above 0 °C). For the measured value of $dE_g/dT = -0.28$ meV/K, the calculated minimum occurs at about -30 °C, whereas the measured one is at -60 °C. Only a further reduction of dE_g/dT leads to a reproduction of the measured minimum of the threshold current. This deviation can be caused by an internal heating of the active region even in pulsed operation and/or by an additional temperature dependence of the surface leakage current.

To further address the question of gain offset effects, simulated curves $N_{th}(T)$ are shown in Fig. 11 for different RT gain offsets $\lambda_p - \lambda_e$ that correspond to the measurements in Fig. 9. A change of the gain offset toward negative numbers at room temperature ($\lambda_e = 1557$ nm) actually shifts the minimum of $N_{th}(T)$ to higher temperatures but it also increases this minimum value. There are several reasons for the rising minimum: the gain is smaller and IVBA is larger at higher temperatures, and the DBR reflectivity becomes smaller for larger wavelength offset.

Fig. 12 shows the measured threshold current at RT as a function of the offset between cavity mode and PL, $\lambda_{PL} - \lambda_e$. A minimum occurs in a region of a detuning between -5 nm and $+5$ nm, i.e., the minimum threshold current at RT is connected with a small offset at this temperature. In this case, the minimum $N_{th}(T)$ still occurs at much lower temperature near -30 °C in the calculation and -60 °C in the measurement, respectively.

The ability to describe the observed behavior is important to design the temperature sensitivity of the VCL. For instance, minimum threshold current at RT might be reached at the expense of a stronger temperature dependence, since the slope

of the curves in Fig. 9 is quite steep at this temperature. Moving the minimum to a higher temperature will increase threshold current, but reduce the temperature sensitivity of the threshold current.

VIII. CONCLUSION

We have fabricated 1.54- μm VCL's with an InP-based integrated bottom mirror and a dielectric top mirror. The lasers were designed for pulsed operation. The temperature performance of the devices, in particular of the threshold current, was investigated. Although a surface leakage channel occurs which is difficult to model, the experimentally observed behavior is described well by a model based on kp band structure calculations and a transfer matrix method. The recorded $I_{\text{thr}}(T)$ characteristics show that the minimum in temperature does not occur for perfect matching of the gain peak and the cavity mode. Therefore, the lowest threshold current for RT is not reached when the minimum is at RT. Anyway, for minimum I_{thr} at RT the gain peak has to match the cavity mode at this temperature. The model is a tool to tune the lasers for, e.g., low threshold current or reduced temperature sensitivity.

REFERENCES

- [1] D. Babic, K. Streubel, R. P. Mirin, N. M. Magalit, J. E. Bowers, E. L. Hu, D. E. Mars, L. Yang, and K. Carey, "Room-temperature continuous-wave operation of 1.54 μm vertical-cavity lasers," *IEEE Photon. Technol. Lett.*, vol. 7, pp. 1225–1227, Nov. 1995.
- [2] J. Piprek, D. I. Babic, and J. E. Bowers, "Numerical analysis of 1.54 μm double-fused vertical cavity lasers operating continuous wave up to 33°C," *Appl. Phys. Lett.*, vol. 68, pp. 2630–2632, May 1996.
- [3] G. P. Agrawal and N. K. Dutta, *Semiconductor Lasers*. New York: Van Nostrand Reinhold, 1993.
- [4] C. H. McMahon, J. W. Bae, C. S. Menoni, D. Patel, and H. Temkin, "Detuning of the gain and reflectivity spectra and its effect on the output characteristics of vertical cavity surface emitting lasers," *Appl. Phys. Lett.*, vol. 66, pp. 2171–2173, Apr. 1995.
- [5] J. W. Scott, S. W. Corzine, D. B. Young, and L. A. Coldren, "Modeling the current to light characteristics of index-guided vertical-cavity surface emitting lasers," *Appl. Phys. Lett.*, vol. 62, pp. 1050–1052, Mar. 1993.
- [6] B. Young, J. W. Scott, F. H. Peters, M. G. Peters, M. L. Majewski, B. J. Thibeault, S. W. Corzine, and L. A. Coldren, "Enhanced performance of offset-gain high-barrier vertical-cavity surface-emitting lasers," *IEEE J. Quantum Electron.*, vol. 29, pp. 2013–2021, 1993.
- [7] B. Tell, K. F. Brown-Gowbeler, R. E. Leibenguth, F. M. Baez, and Y. H. Lee, "Temperature dependence of GaAs–AlGaAs vertical cavity surface emitting laser," *Appl. Phys. Lett.*, vol. 60, pp. 683–685, Feb. 1992.
- [8] N. M. Margalit, D. I. Babic, K. Streubel, R. P. Mirin, D. E. Mars, J. E. Bowers, and E. L. Hu, "Laterally oxidized long wavelength cw vertical-cavity lasers," *Appl. Phys. Lett.*, vol. 69, pp. 471–472, July 1996.
- [9] K. Streubel, S. Rapp, J. Andre, and J. Wallin, "Room-temperature pulsed operation of 1.5 μm vertical cavity lasers with an InP-based Bragg reflector," *IEEE Photon. Technol. Lett.*, vol. 8, pp. 1121–1123, Sept. 1996.
- [10] K. Streubel, J. Wallin, G. Landgren, U. Öhlander, S. Lourudoss, and O. Kjebon, "Importance of metalorganic vapor phase epitaxy growth conditions for the fabrication of GaInAsP strained quantum well lasers," *J. Cryst. Growth*, vol. 143, pp. 7–14, 1994.

- [11] J. Piprek, D. I. Babic, N. M. Margalit, and J. E. Bowers, "Loss analysis of 1.55 μm vertical cavity lasers," in *Proc. 15th Int. Conf. Semiconductor Lasers*, Haifa, Israel, 1996, pp. 25–26.
- [12] J. Piprek, D. I. Babic, and J. E. Bowers, "Modeling and optimization of 1.54 μm double-fused VCSELs for cw operation above room temperature," *SPIE*, vol. 2693, pp. 149–156, 1996.
- [13] J. Piprek, "High-temperature lasing of long-wavelength VCSELs: Problems and prospects," in *SPIE Proc.*, 1997, vol. 3003, pp. 182–193.
- [14] W. W. Chow, S. W. Corzine, D. B. Young, and L. A. Coldren, "Many body effects in the temperature dependence of threshold in a vertical-cavity surface-emitting laser," *Appl. Phys. Lett.*, vol. 66, pp. 2460–2462, 1996.



Stefan Rapp received the M.S. degree in physics from the University of Stuttgart, Germany, in 1994. He is currently pursuing the Ph.D. degree at the Royal Institute Technology (KTH), Stockholm, Sweden. His doctoral research concerns vertical-cavity surface-emitting lasers for long-wavelength operation.

Joachim Piprek (M'94), for photograph and biography, see p. 1383 of the August 1997 issue of this JOURNAL.

Klaus Streubel received the diploma and the Ph.D. degree in physics from the University of Stuttgart, Germany, in 1985 and 1991, respectively. His doctoral research involved the MOVPE growth of GaInAs–InP quantum-well structures and the study of quantum-well interfaces.

In 1991, he joined the Swedish Institute of Microelectronics, Stockholm, Sweden, working on the fabrication and characterization of strained and strain-compensated GaInAsP–InP quantum wells for laser applications. Since 1993, he has been employed by the Royal Institute of Technology (KTH), Stockholm, as a Research Staff Member. Currently he is working on vertical-cavity surface-emitting lasers for long-wavelength operation.

Dr. Streubel is member of the German Physical Society (DPG), the German Society for Crystal Growth (DGKK), and the IEEE Lasers and Electro-Optics Society (LEOS).



Janos André was born in Hungary in 1944.

He worked with Si-vapor phase epitaxy at Tungsram in Budapest, Hungary. From 1970 through 1994, he worked as an Engineer at the Swedish Institute for Microelectronics (IM) in Stockholm, Sweden. Since 1994, he has been with the Royal Institute of Technology, Stockholm. He is mainly involved in the process technology of III–IV semiconductor devices.

J. Wallin, photograph and biography not available at the time of publication.